RESEARCH ARTICLE

Mebendazole Loaded Nanoparticles for Lung Cancer Therapy

Heba Anaaa, Frezah Muhanab, Mohamed El-Tanania*, Razan Madic, Rahmeh Kerfanc

Phamacologic and Diagnostic Research Center(PDRC), Al-Ahliyya Amman University, Amman, Jordan

Received: 1st August, 2022; Revised: 28th August, 2022; Accepted: 3rd September, 2022; Available Online: 25th September, 2022

ABSTRACT

Lung cancer is the leading cause of cancer mortality. Lung cancers are classified into two types based on their microscopic appearance: small cell lung cancer (SCLC) and non-small cell lung cancer (NSCLC). Many individuals are first diagnosed at stage III or IV, when their prognosis is bleak. Non-small cell lung cancer is a lethal and incurable illness that can be treated with surgery, chemotherapy, radiation therapy, targeted therapy, or a combination of therapies. Targeted treatment focuses on particular abnormalities seen in cancer cells, such as the Epidermal growth factor receptor (EGFR) mutation. The T 790M mutation in the EGFR's tyrosine kinase domain causes acquired resistance to first-generation EGFR TKIs, mebendazole. As a result, combining diverse targeted therapeutic drugs not only improves treatment outcomes but can also be a more effective preventer of acquired resistance improvement. Loaded drug Nanoparticles ZSM-5 and SBA-16 were utilized as targeted treatment, and their stability and loading % were determined using multiple methods, including infrared, X-Ray Diffraction, TGA, and HPLC. The therapy was used in in-vitro cell culture investigations such as the MMT assay, colony assay, and migration assay. The results showed that the loaded drug nanoparticles had a lower IC_{50} than the free drug mebendazole we utilized, indicating that the nanoparticles improved therapy and reduced medication dosage.

Keywords: Anticancer, Medication, Mebendazole, Nanoparticle, SBA 16 nanoparticle, ZSM 5.

International Journal of Drug Delivery Technology (2022); DOI: 10.25258/ijddt.12.3.22

How to cite this article: Anaaa H, Muhanab F, El-Tanania M*, Madic R, Kerfanc R, Mebendazole Loaded Nanoparticles for Lung Cancer Therapy. International Journal of Drug Delivery Technology. 2022;12(3):1053-1065.

Source of support: Nil.

Conflict of interest: None

INTRODUCTION

Lung cancer is the leading cause of cancer death in both men and women.[1] Small cell lung cancer (SCLC) or oat cell cancer accounts for 15–20% of all instances and is the most aggressive kind.[2] Non Small Cell Lung Carcinoma (NSCLC) is the most prevalent kind of lung cancer, accounting for 80–85% of cases. NSCLC comes in three forms. Adenocarcinoma, Squamous cell carcinoma (SCC) and Large-cell carcinoma (LCC). Subtypes of lung cancer, notably NSCLC, can spread to other organs. Early NSCLC frequently has no respiratory symptoms, avoiding diagnosis.[3-5] Stage III or IV diagnosis with poor prognosis and low progression-free survival rate.[6,7] Despite significant therapeutic advances in the recent decade, advanced lung cancer is lethal and incurable.[8,9] Non-small cell lung cancer is treated with surgery, chemo, radiation, targeted therapy, or a combination of these.[10,11] Various medicines have been improved to block tumor development, growth, metastasis, and angiogenesis.[12,13] Small molecule tyrosine kinase inhibitors stand out among these newer medicines (TKIs).[14] Despite the high success rate of targeted therapy, most cancers become resistant within a year. On-target and off-target resistance to targeted treatment exist in NSCLC.[15] Oncogenic kinases including Epidermal growth factor receptor (EGFR), Anaplastic lymphoma kinase (ALK), and ROS Proto-Oncogene 1 (ROS1) mutations are well-known drug resistance mechanisms in several NSCLC subtypes. In the tyrosine kinase domain, the T790M mutation leads to acquired resistance to first generation EGFR TKIs.[16] Thus, combining targeted therapeutic drugs can not only improve treatment outcomes but also avoid the development of acquired resistance.[17] This is the main premise of the *in-vitro* research and will be discussed in depth in the experimental phase.[18] RTKs are a kind of growth factor receptor that has tyrosine kinase activity.[19] Examples include the Epidermal growth factor receptor (EGFR), Fibroblast growth factor receptor (FGFR), Platelet-derived growth factor receptor (PDGFR), Hepatocyte growth factor receptor (HGFR), Special function register (SFR), Methionine (MET), Vascular endothelial growth factor (VEGFR), EPH receptors, and insulin receptor (INSR).[20]

Ran is also known as GTP binding protein.[19] First identified in the nucleocytoplasmic transport of macromolecules through the nuclear membrane, A recent study found it important in mitotic spindle formation and postmitotic nuclear assembly.[20] This is important because Ran, like other GTPases, alternates between the inactive GDP and active GTP bounds.[21] Guanine nucleotide exchange (GEF) transports proteins and

Author for Correspondence: fhmuhana@gmail.com

ribonucleoprotein molecules across the nuclear pore complex (RCC1). Notably, ran has a role in mitosis.[22] Its method of action is similar to that of nucleocytoplasmic shuttles,[23] and current study reveals its participation in many spindle targets. The activation of Ran GTPase is critical for cell survival.[24,25] A Ran system disorder can produce a succession of mitotic mistakes, causing a cell to become genetically unstable.[26,27] Because genomic instability might cause cancer growth, Ran's role in the oncogenic pathway has been determined. The expression of Ran GTPase has been linked to the onset and development of cancer.[28,29] Multifunctional nanovesicles have recently been a major focus of bio-nano-medicine research for medication delivery.[30,31] A nanocarrier should serve as a drug carrier, delivering its load to the target tissue with sustained activity.[32] These nanostructures must have specific structural properties for targeted therapy: identifying, distinguishing, and treating cancerous cells. TEOS is first hydrolyzed in acid, then polymerized to produce a cubic mesoporous structure with linked mesopore chambers and channels.[33] SBA-16 has a large pore size, thick pore walls and a high thermal stability.[34] Therefore, it has been employed in catalysis, adsorption of metal ions, electronics and drug delivery.[34]

ZSM-5 and SBA-16 nanocarriers have been utilized to transport water-soluble medicines.[35] This form of aluminosilicate is composed of fundamental building blocks of tetrahedral $[SiO4]^{4-}$ and $[AlO_3]^{4-}$ connected by oxygen atom corner sharing (oxygen bridges)[36] The SiO_4 tetrahedra is balanced, while the AlO4 tetrahedra is negative.[37] Overall, zeolites have the following chemical formula.[38] (M_2/nO.Al_2O_3.$ySiO_2$.wH_2O) in zeolite. where M is an n-charged cation that counteracts the negative charge of $[AlO3]^{4-}$ tetrahedra. Aluminosilicate minerals include zeolites.[39,40] Their channels and cavities have nanoscale molecular architectures. This characteristic makes them dimensional selective, i.e., they restrict molecules of the same dimension from entering but enable molecules of other dimensions to pass.[41] Acidic sites are another feature.[42] The pores and channels allow tiny molecules to be encapsulated.[43] The purpose of this work is to describe the effective synthesis of ZSM-5 and SBA-16 nanocarriers for loading the sparingly soluble anticancer medication mebendazole. Additionally, results demonstrated significant reduction of Ran mRNA of up to 40% in the A549 cell line, which was consistent with previously published data on vincristine for the treatment of glioma and DOX for the treatment of lung metastasis.[41,42]

MATERIALS AND METHODS

Chemicals

Tetrapropyl ammonium hydroxide ($C_{12}H_{29}NO$) sigma Aldrich – Switzerland. Tetraethyl orthosilicate ($C_8H_{20}O_4Si$) sigma Aldrich – china, Aluminum sulfate hydrate ($AL_2O_{12}S_3$.XH_2O) sigma Aldrich – USA, Sodium hydroxide, Sigma Aldrich – Sweden. Pluronic sifma ldrich – USA. Hydrochloric acid scharlab – European, Calcium chloride anhydrous TIMSTAR – U. K. Toluene. tedia – USA.Molecular sieve Riedel de haen, Isopropanol sigma Aldrich – France. 3-aminopropyl triethoxysilane sigma Aldrich – china. Sodium phosphate monobasic dehydrate acros, Disodium hydrogen orthophosphate dodecahydrate GPR. Melt-2015) DMEM. Media euroclone. Italy. PBSeuro clone. Italy. Fetal bovine serumeuro clone. Italy. Penicillin euro clone. Italy. Streptomycin.euro clone. Italy. Trypsin euro clone. Italy. Trypan blue dye. GCC, U. K. Solubilization solution / Stop mix Promega – USA. (Yellow dye) 3-(4,5-dimethylthiazol-2-yl)-2,5-diphenyl tetrazolium bromide Promega – USA DMSO GCC – U. K. Acetonitrile Tedia-America. Sodium lauryl sulfate Tedia-America. Phosphoric acid Tedia-America. Formic acid Tedia-America. Methano Tedia-America. Monobasic potassium phosphateTedia-America Triblock copolymer (PEO20PPO70PEO20) was purchased from Acros Organics, New Jersey, US. Tetraethylorthosilicate (TEOS) was purchased from Aldrich, St. Louis-US. mebendazole was kindly supplied by Pharma International, Jordan. Sodium hydroxide pellets (BDH, City Road, London), hydrochloric acid 35% (SD Fine-Chem Limited, Mumbai-India), and absolute ethanol 99.8% (AZ Chem, Pretoria-South Africa) were used as received. Hydrochloric acid 95% (Merck, New Jersey-US) was used to clean all glass equipment before us.

Preparation of Zeolite ZSM-5 Nanoparticles

To a 50 mL solution containing 12.0 g tetrapropylammonium hydroxide, 12.0 g tetraethyl orthosilicate was added. Following that, place the flask containing the solution in a water bath/shaker. The mixture was diluted with a sufficient amount of aluminum sulfate hydrate 0.722 g, sodium hydride 0.24 g, and deionized water 4.0 g after 24 hours at 80ºC. Placing the mixture in a Teflon-lined autoclave and heating it to 170°C for 24 hours to crystallize. The gel's molecular makeup will be as follows: 100 Al2O3: 0.25 TPAH: 0.5 Na2O: 50 H2O 1 SiO2: 100 Al2O3: 0.25 TPAH: 0.5 Na2O: 50 H2O Finally, the mixture will be centrifuged and calcinated at 550ºC for six hours.[45]

Preparation of SBA-16 Nanoparticles

SBA-16 nanocomposites were produced following Thomas's approach, with slight alterations. 4.0 g pluronic F127 was typically dissolved in 30 mL water and 120 mL 2 M HCl solution while stirring regularly. Then, 9.1 mL TEOS was added while stirring at 35ºC. After another 20 hours of stirring, the mixture was aged overnight without stirring in a water bath set at 80ºC. The product was collected using gravity filtering and then washed with deionized water and air dried overnight at 100ºC. The surfactant was removed using calcination at 550ºC for 6 hours.[36]

Preparation of coupling SBA-16 and ZSM-5 nanoparticles

SBA-16 and ZSM-5 nanoparticles with an amine functional group. Functionalization was accomplished by the application of a previously described technique. To eliminate adsorbed water, one gram of silicate material was dried overnight at 110ºC. Stirring was employed to disseminate the silicate

sample in 50.0 mL toluene, followed by the addition of APTES (10 mmol). Under nitrogen, the mixture was reflux heated for 12 hours. Filtration and washing with 3.50 mL toluene, followed by isopropanol, were performed on the resulting product (3.50 mL). Vacuum drying of the functionalized silicate material at 60ºC for 12 hours. The increased reaction precursor ratios stated before assisted in increasing the functionalization %. The silicalite-1-NH2 functionalized products were termed silicalite-1-NH2.[46,47]

Characterization of the prepared nanoparticles

Synthesis of ZSM-5 and SBA-16 Nanoparticles

The percentage yield was 3.00 g and 2.89 g of ZSM-5 and SBA-16, respectively. Powder of all nanoparticles were white, uniform size (after sieving) and the formation of product was 2.5.2 confirmed using zeta potential, SEM, FT-IR and XRD as described in the characterization section below.

Zeta Potential Analysis and Scanning Electron Microscope

In order to determine the surface of various nanoparticles, the zeta potential of all samples was determined by photon correlation spectroscopy using a Nano-Zetasizer (Malvern Instruments, Nano ZS, UK) working on the dynamic light scattering platform equipped with a standard 633-nm laser and the size was confirmed by Scanning electron microscope (SEM, TECAN MIR3 FEG) was used to observe the morphology of the mesoporous nanocarriers.

Thermal Gravimetric Analysis (TGA)

Thermogravimetric analysis of the ZSM-5, coupling ZSM-5,mebendazole, and loaded drug were done using a NETZSCH STA 409 PC instrument (NETZSCH, Germany) with a 20 mL/min N_2 gas purge flow and a 20°C/min scan rate. For each run, a sample (10 mg) was placed in a hermetically sealed aluminium pan with a pinhole. After equilibration at 25°C, the sample cell was warmed to 1000°C. Indium metal was used as the calibrating reference.

PXRD Data for Mebendazole

Nanoparticles SBA-16, and ZSM-5 were recorded in transmission geometry with Cu-K radiation (= 1.5406 A) at 40 kV/100 mA using a Shimadzu XRD-7000 diffractometer (Japan). The samples were prepared on deep silicon single crystal sample holders measuring 20 mm in diameter. At a temperature of 25°C, each sample was measured between 2 = 5° and 50° using a step and scan rate of 2°/min.

Fourier Transfer Infra-red (FT-IR)

Each sample of mebendazole, SBA-16 and ZSM-5 nanoparticles, drug, and loaded drug (1-mg) was ground into a powder with dried KBr (50 mg) in a mortar and the mixture was pressed into a slice. The FT-IR spectra were recorded in the range of 4000–400 cm^{-1} using a Thermo Nicolet NEXUS 670 FT-IR spectrometer.

Drug Loading on ZSM-5 and SBA-16 Nanoparticles

HPLC Method of Analysis of Mebendazole

The peak represents mebendazole appeared at retention time equals to 3.4 min with a resolution more than 5. (Figure 1A) shows the chromatogram of mebendazole.

Linearity and Calibration Curve of Mebendazole

Mebendazole linearity was obtained in concentration range between 20–100 µg/mL. Although The International Council for Harmonisation of Technical Requirements for Pharmaceuticals for Human Use (ICH) guideline set six concentrations as a minimum requirement, in this test 9 concentrations gave a high correlation coefficient. (Figure 1A) illustrate the calibration curve of pure mebendazole which was done by plotting the measured area vs. concentrations. The linearity R^2 was equals to 0.9978 which complies with the ICH guideline.

Physical adsorption is used to load guest molecules onto mesoporous silica. To load mebendazole into samples of mesoporous SBA-16, the following procedure was used: mebendazole (0.100 g) was suspended in water (25.0 mL) and then added to a flask containing mesoporous SBA-15 (0.100 g). The combination was blended in the dark at room temperature for 24 hours. Filtration and vacuum drying of the solid component of the drug-loaded carrier for 2 hours at 60°C (30 mmHg).

Drug Release from Nanoparticle

This test was performed using ERWEKA dissolution test apparatus Type II (paddle) as described by the United States Pharmacopoeia. The media was prepared using 9 mL of HCl and completed to 1.0 L by distilled water then the pH was adjusted to 0.1 M using sodium hydroxide and HCL. Then 900 ml of media was added to each jar in the ERWEKA dissolution tester and left for 1-hours at 37ºC, 50 rpm before adding the drug to equilibrate with temperature. After 1-hour, a 0.05 g of pure drug powder was added to three jars, 0.11 g of ZSM-5 loaded drug which is equivalent to the required amount of drug was added to another three jars and 0.11 g of SBA-16 loaded drug was added to another 3 jars. Samples were taken at time intervals 5, 15, 30, 40, 50, 60 and 75 minutes, 5 mL from each jar was taken and replaced with 5 mL of fresh media. Then each sample was diluted 1:1 using mobile phase and the concentration of dissolved carvedilol was determined using HPLC method.

MTT Assay

The ATTC A-549 cell line was grown according to normal methods. A-549 cells passage 53 were planted in T75 flasks with 1% penicillin-streptomycin and 10% fetal bovine serum in Dulbecco's Modified Eagle Medium (DMEM) (FBS). Cells were incubated at 37°C in a 5% CO_2 environment. Euro-clone provided all chemicals utilized in cell culture.[48]

IC50 Determination

IC50 was determined using the MTT Cell Proliferation Assay as following: In 96-well plate, 10,000 cells in 100 µL of DMEM

medium were cultured in each well then, the plate was placed in a CO_2 incubator at 37°C for 24 hours. After that the media were removed from the wells and different doses (100 nM, 200 nm, 300 nm, 500 nm and 700 nm) of mebendazole, ZSM-5 and loaded drug and DMSO (as negative control) were prepared each in 100 µL medium and added to wells then the plate was incubated in humidified 5% CO_2 incubator at 37°C for 24 hours after that 1-mL of MTT reagent was added to 10 mL of DMEM media then 110 µL of previous media and MTT reagent was replaced the media on each well followed by incubation at 37°C in 5% CO_2 and 95% humidity for 4 hours, then 85 µL of media was discharged from each well followed by adding 50 µL DMSO. Then after 10 minutes the absorbance was recorded at 590 nm using a Biotech 96-well plate reader. Finally, the IC_{50} value was determined using Prism-Graphpad.[48]

Scratch-migration Assay

The migratory and proliferative characteristics of the A539 cell lines were determined utilizing a scratch wound test.[48] Cells were grown in Dulbecco's modified Eagle medium (DMEM) containing 10% fetal bovine serum (FBS) and incubated at a CO_2 concentration of 5% and a relative humidity of 95%. For 24 hours at 37°C, 3 105 cells/mL were seeded into 96-well tissue culture plates containing poly lysine-coated cover slips (Thermo Fisher Scientific Inc., USA). A linear wound was made using a sterile 100 L plastic pipette tip when cultivated cells form confluent monolayers. To eliminate any cellular debris, the cover slips were rinsed with phosphate buffered saline (PBS). Two control groups were used: a negative control group was given DMEM medium containing 0.25% DMSO, while a positive control group was given (10 nM) DMSO in media. The formulation ZSM-5 was found to be loaded with Melt-2015 (IC_{50} values of 0.41 M were utilized). The scratch's surface area was measured at zero time, which is when it was performed, and also 24 hours afterwards. Three sample photos of each coverslip's scratch region were used to determine the relative migration of cells under each condition. The data were analyzed using Motic software version 2 (Motic China group Co. LTD). At least three replicates of each experiment were carried out. The closure rate was determined using the following formula supplied by the CytoSelectTM 24-well wound healing test (Cell Biolabs, INC, USA)in equation one.[49]

Ribonucleic Acid (RNA) Extraction and Analysis

The RNeasy Mini kit was used to extract total RNA (QIAGEN, USA). Cell pellets were frozen on ice and resuspended in a 500 L lysis solution containing 2-mercaptoethanol. To eliminate cellular debris, an equivalent amount 500 L of 70% ethanol solution was added to the filtered lysate and vortexed completely. The lysate was then transferred to the RNeasy Mini spin column and spun at 10000 rpm for 15 seconds using a microcentrifuge. The binding column was used to capture whole RNA. The liquid from the flow-through was discarded, and the collecting tube was reintroduced into a binding column. The washing procedure was performed three times.

Following that, the binding column was moved to a new collection tube. 50 L of RNase-free water was added directly to the spin column membrane as an elution solution and centrifuged at 10000 rpm for 1-minute to elute the RNA. Purified RNA was promptly kept at -80°C. A NanoDrop ND-1000 spectrophotometer was used to evaluate the concentration and purity of the extracted total RNA (Thermo Scientific, Wilmington, USA). The optical densities at 260 and 280 nm were found. For the majority of the RNA extracted samples, the ratio (A260/A280) was between 1.8 and 2.1.[50]

$$\text{Closure percent} = \frac{\text{surface area after 24 h}}{\text{surface area at 0 time}}\ x\ 100\% \quad \text{.....}$$

Complementary Deoxyribonucleic Acid (cDNA) Synthesis

The reverse transcription technology was used to produce cDNA (Applied Biosystem, USA). 2 g total RNA was combined with 1 L-oligodeoxythimidine primer in a microcentrifuge tube and incubated for 5 minutes at 65°C using a thermocycler C 1000 (Bio-Rad, USA). The tubes were quickly centrifuged and stored on ice. The following reagents were added to the 20 L reaction solution: 1.4 L of 25 mM magnesium chloride, 4 L of a 10 mM deoxynucleotide triphosphate (dNTP) combination Reverse transcription 10x buffer (2L), recombinant RNasin® ribonuclease inhibitor (1L), reverse transcriptase from avian myeloblastosis virus (1L) (AMV-RT). The following temperature settings were used to synthesize cDNA: For 30 minutes, microcentrifuge tubes were incubated at 37°C. Denaturation was accomplished by heating samples to 95°C for 5 minutes. After 5 minutes at 4°C, microcentrifuge tubes were incubated and kept at -80°C for future analysis. NanoDrop ND-1000 spectrophotometer was used to evaluate the concentration and purity of cDNA (Thermo Scientific, Wilmington, USA). The optical densities at 260 and 280 nm were found. For the majority of the cDNA extracted samples, the ratio (A260/A280) was 1.6–1.8.[48]

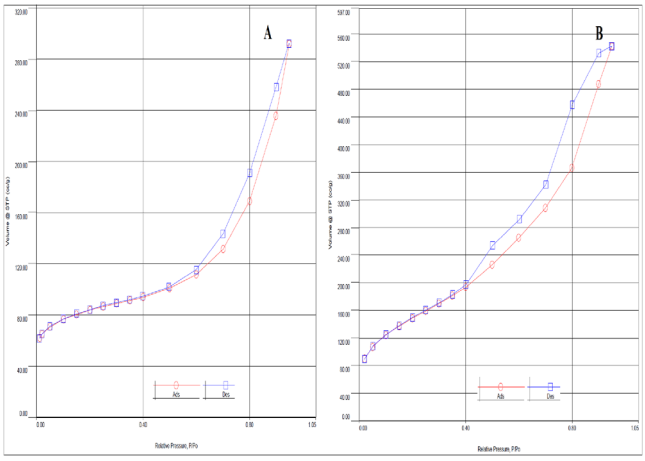

Figure 1: Nitrogen adsorption/ desorption isotherm of (A) ZSM-5 and (B) SBA-16 to determine the pore size and surface area were estimated of ZSM-5 (1.232 nm, 360.1 m^2l/g) and SBA-16 93.627 nm, 615 m^2/g).

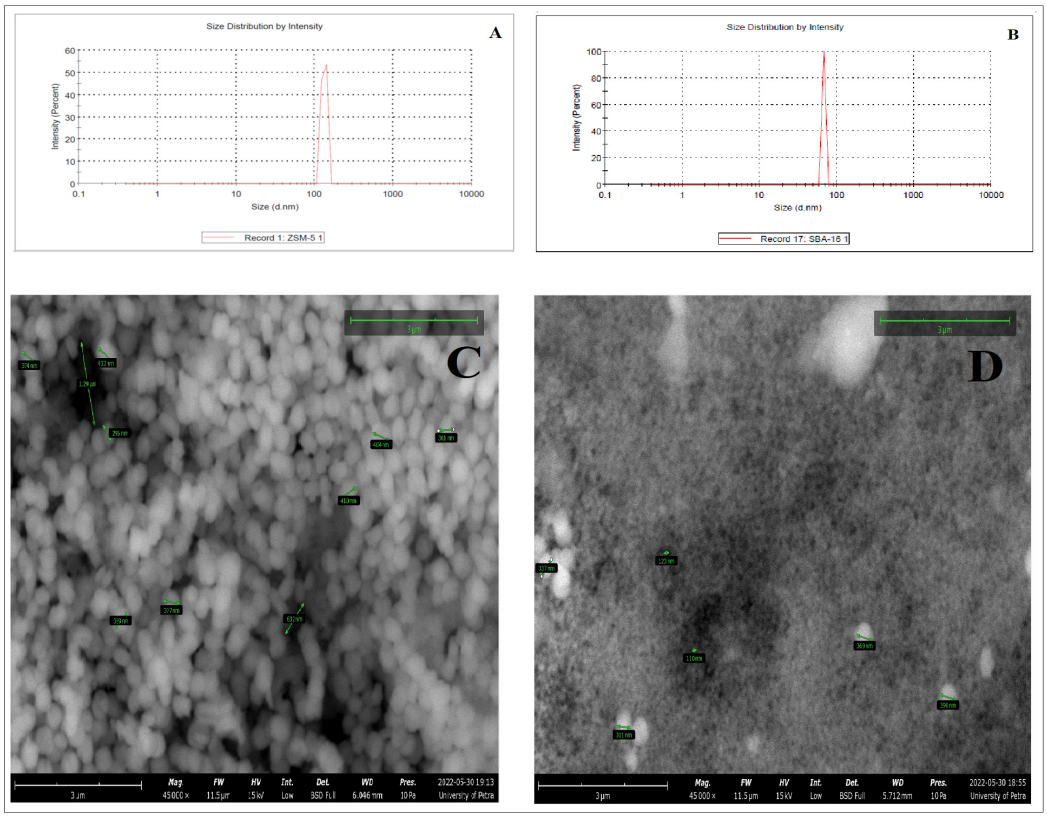

Figure 2: (A) Zeta potential of ZSM-5, B) SBA-16 that measured the size and the PDI values of ZSM-5 and SBA-16 formulations to be equal 132.8 nm ± 9.600 and 68.06 nm ± 0.000, respectively. and SEM of (C) ZSM-5, (B) SBA-16 which indicated that all micrographs depict homogeneous distribution of particles

Real-time Polymerase Chain Reaction

RNA was extracted using selective binding to silica-based membranes (RNeasy® Mini Kit, Qiagen Ltd., Manchester, UK), and reverse transcription was performed using SuperScriptTM III first-strand synthesis system (Invitrogen Ltd.) according to the instructions supplied by the manufacturer. Real-time PCR (Applied Biosystem, Foster City, CA) was performed using an SYBR® Green assay for RanGTP and a forward primer 5' CCATCTTTCCAGCCTCAGTC 3′ and reverse primer 5'CCAAGGAAGGCGTCTAAGGC 3'.[48]

RESULTS AND DISCUSSION

Characterization of ZSM-5 and SBA-16

N2 Adsorption/ desorption isotherm, PDI, Zeta Potential and Scanning Electron SEM) Characterizations of the Synthesized nanoparticles and success of loaded were examined by TGA (Thermogravimetric analysis), IR (infrared) and XRD (X-Ray Diffraction).

NC Adsorption/Desorption Isotherm

Nitrogen adsorption/desorption isotherms were used to estimate the average pore diameter (nm) and specific surface area (m^2/g) for ZSM-5 and SBA-16 nanoparticles (Figure 1ABC). The adsorption isotherm was used for the estimation of surface area by applying Brunauer-Emmett-Teller (BET) theory, while the desorption isotherm was used to estimate the average diameter of the pores by applying Barrett-Joyner-Halenda (BJH) theory. The pore size and surface area were estimated of ZSM-5 (1.232 nm, 360.1 m^2/g)[51] and SBA-16 (3.627 nm, 615 m^2/g) all these results are close to what has been reported in the literature.[52]

PDI, and Zeta Potential and Scanning Electron Microscopy

Characterizations of the Synthesized nanoparticles. The size, PDI, and zeta potential of the new nanoformulations were also measured. The results demonstrated that ZSM-5 and SBA-16 formulations were synthesized in nanoscale dimensions with the size of 132.8 nm ± 9.600 and 68.06 nm ± 0.000, respectively. Moreover, the PDI values of the nanoparticles were found to be in of ZSM-5 and SBA-16 0.317 and 0.039. (Figure 2C). The particle size and PDI are critical factors to determine the efficacy of nanoparticles as drug carriers.[53,54] nanoparticles with PDI values as mentioned above are monodisperse morphology and homogenous.[55] In other hands, particles morphology and size were confirmed also by the scanning electron microscopy (SEM). Estimates of the sizes of ZSM-5 was obtained through SEM micrographs. All micrographs depict homogeneous distribution of particles, some of the particles have elongated cubic shapes while others have hexagonal prismatic units with particle size distributions in the range of 0.4–0.8 μm. While the SEM images of the SBA-16 synthesis led to a mixture of

cubic, faceted and spherical particles with diameters around 5.0 µm (Figure 2 CD).

TGA Analysis

TGA analysis was used to characterize mebendazole and the nanoparticles that were created (Figure 3 A-D). As depicted in the graph, ZSM-5 nanoparticles lost 2.48% of their mass upon heating to 1000°C. This weight loss was attributed to the evaporation of water molecules, indicating that nanoparticles are thermally stable and hydrophilic. These characteristics indicated their suitability for loading hydrophobic mebendazole drug molecules.[56,57] In addition, the results demonstrated that mebendazole began to lose weight at ~212°C and continued to do so until it was completely decomposed at 80°C. The drug-loaded nanoparticles exhibited a weight loss of 49.23%, which corresponded to their drug-loading capacity. It was observed that the weight loss of ZSM5-NH2 began at 160°C and plateaued at 550°C The presence of the grafted amino group on the nanoparticles' surfaces resulted in a 12.66 % decrease in the total weight of the grafted nanoparticles.

X-Ray Diffraction (XRD)

The XRD spectrum (Figure 2 ABCEFG) confirms the crystallinity and purity of the MFI ZSM-5 structure, drug, and loaded drug. The XRD pattern of SBA-16 mesoporous, drug-loaded material (Figure 4A) reveals a peak for at 2 of 0.7 degrees, which is consistent with previous reports in the literature.[45] As seen by strong and powerful diffraction peaks, the XRD patterns of pure mebendazole raw material reveal crystalline material. The XRD patterns matched those described by Thomas, and his study team (2010).[58] The crystal structure of pure mebendazole has been reported to have strong peaks at (7.59 and 17.27, 19.73, 26.78, 38.0 and 44.0). Analyses of carriers containing drugs The XRD spectrum verifies the loading of mebendazole with a unique peak appearance at the XRD loading pattern of the medication, while simultaneously disappearing the two primary peaks at 2 of 40. This is a sign of mebendazole crystallization within the nanocarriers' pores. The considerable drop in the crystalline characteristic peaks of loaded mebendazole, on the other hand, showed a less ordered crystallinity than that of the pure drug. This resulted in a reduction in crystallinity. Previous research indicated that larger drug loadings of roughly 50% (w/w) might be attributed to partial amorphization, with a tiny quantity of crystalline

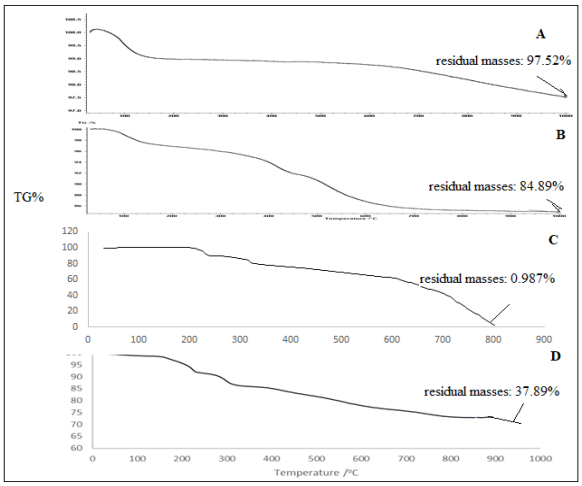

Figure 3: (A) TGA of ZSM-5 is showing thermal stability, (B) of Coupling ZSM-5 is showing decrease in the value of residual mass due to successful coupling with 3-aminopropyltriethoxysilane, (C) drug, (D) Loaded drug.

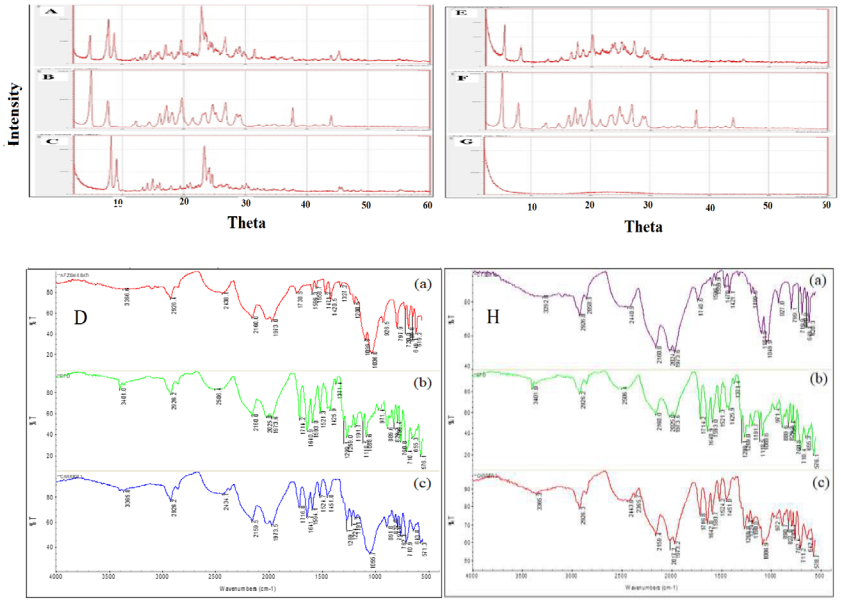

Figure 4: XRD of A) ZSM-5, B) mebendazole and C) Loaded drug and this also confirmed by Infrared in D) where a) ZSM-5, b) mebendazole and c) Loaded drug and this is the same for the XRD second carrier E) SBA-16, F) mebendazole and G) Loaded drug and this also confirmed by Infrared in H) where a) SBA-16, b) mebendazole and c) Loaded drug.

drug remaining on the produced particles' external surface. Similarly, connecting ZSM-5 and SBA 16 nanoparticles produced X-ray patterns similar to the origin nanocarrier structure, but with a drop in peak intensity and a small shift to lower values of 2y, showing that the ZSM-5 and mesoporous structure remained consistent during functionalization as seen in (Figure 4).[58,59]

Fourier Transform Infrared Spectroscopy (FT-IR)

To get a better understanding of the interaction between mebendazole and mesoporous SBA-16, zeolite ZSM-5 nanoparticles, both alone and in combination with medication, FT-IR spectra were obtained for mebendazole and SBA-16, ZSM-5, and loaded nanocarriers. Supplementary Tables 1 and 2 provide the bands required for nanocarrier assignment, whereas Supplementary Table 3 includes the bands required for drug and loaded drug. FTIR spectra were acquired throughout the range 4000–4004 cm^{-1} with a spectral resolution of 4 cm^{-1} using KBr discs. (Figure 5Dabc, Habc) exhibits distinct distinctive bands of nanocarriers, drug, and loaded drug, which are consistent with previously reported data.[60,61] FTIR-spectrometry was used to validate the loading of mebendazole into a Zeolite ZSM-5 nanocarrier (mesoporous SBA-16 and Zeolite nanocarrier exhibit a nearly identical absorption band). Supplementary Table 3 indisputably reveals the presence of mebendazole in the loaded samples. mebendazole's spectra (Figure 5Dabc, Habc) exhibited absorption bands at 3484.324 and 1738.54 cm^{-1}, which correspond to the N-H and C=O stretching, respectively. The presence of an absorption band around 1640.9 cm^{-1} established the presence of the C-N stretching absorption band, whereas the presence of the C=C bond was established by the presence of a stretching absorption band at 1594.1 4 cm^{-1}. (Figure 5Dabc, Habc) and Supplementary Table 3 demonstrates changes in the spectrum of mebendazole's representative peaks in the loaded carrier vibration. The nanocarrier's (O-H) peak superimposed on mebendazole's (N-H) peak in the spectrum, and the carbonyl peaks (C=O), (C-N), and (C=O) at higher energies, indicating intermolecular interactions between mebendazole and the Zeolite ZSM-5 nanocarriers. These spectra established the formation of hydrogen bonds between mebendazole, a hydrogen bond acceptor, and Zeolite ZSM-5 nanoparticles, a proton donor. They might be explained, the drug encapsulation procedure involves the adsorption of the drug to the mesoporous nanocarrier pores/outer surface under physisorption interactions that favor drug-carrier interactions such as van der Waal's interactions, hydrogen bonding, as has been shown before in other systems such as zeolite Y.[62,63] and montmorillonite.[63] When ZSM-5 and SBA 16 were functionalized with an amino group, the Si-OH peak at about 3366.6 cm^{-1} in the unmodified FT-IR spectrum disappeared and new peaks for the propyl backbone (nC-H) developed at roughly 2930 cm^{-1}. Stretching bands projected to form in the 3200–3500 cm^{-1} range as a result of nNH2 were masked by the wide band of adsorbed water (Figure 5 Dabc, Habc).

High Performance Liquid Chromatography (HPLC)

HPLC is primarily used to identify, quantify, and purify the mixture's separate components. HPLC was utilized to evaluate the purification process following the load, and the result included a single peak indicating that the carrier had no influence on the drug as a pure substance throughout the load.

Calibration Curve of Mebendazole

HPLC is primarily used to identify, quantify, and purify the mixture's individual components. HPLC was used to evaluate the purification process after the load, and the result was a single peak, indicating that the carrier no effect on the drug's purity throughout the load.

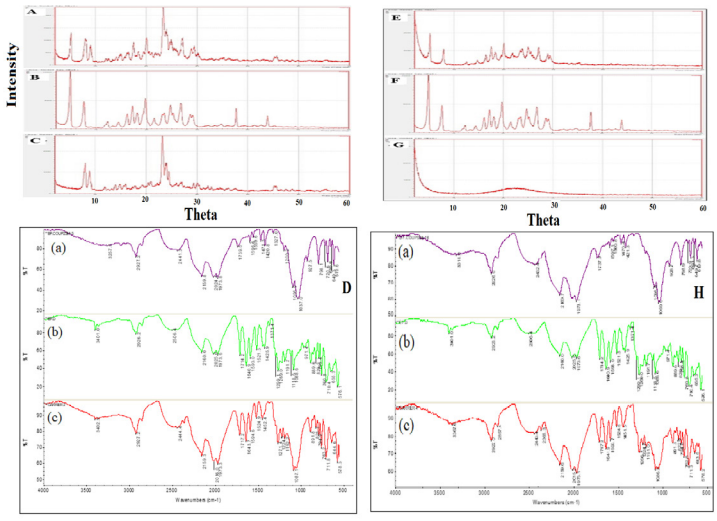

Figure 5: XRD of A) coupling ZSM-5, B) mebendazole and C) Loaded drug and this also confirmed by Infrared in D) where a) coupling ZSM-5, b) mebendazole and c) Loaded drug and this is the same for the XRD second carrier E) Coupling SBA-16, F) mebendazole and G) Loaded drug and this also confirmed by Infrared in H) where a) Coupling SBA-16, b) mebendazole and c) Loaded drug.

Carrier Loading of Mebendazole on ZSM-5 in Buffer Solution

The Y-axis represents the viable cells, while the X-axis represents the average of triplicate treatments at concentrations of 600, 300, and 100 microM. The slope of the Y equation equals IC_{50}, whereas Y=50 indicates a 50% effect of treatment on the cells. IC_{50} values of the drug in its Free form. It has been shown that the IC_{50} of nanoparticulate drug is significantly less than its free form. It has been demonstrated that IC_{50} of nanoparticulate drug is considerably lower than that of its free form. This suggests that the nanoparticles carriers increased the efficacy of the drug and decrease its therapeutic effect. Therefore, when the carriers are used, the medication is more effective than when it is administered without them.

Dissolution Test

In dissolution test, HCL and Buffer solution were utilized as media. Comparing our HCl formulation to that of a commercially available drug reveals that the same percentage of drug was released within the first 15 minutes. and the same release percentage Buffer. There is no published research on the alkaline media release of the drug. This is a good result, as there is no difference between two formulas, but the effect of our formula on biology experiments (cell culture) was superior to that commercial formula, as described in MTT assay result section . as shown in the additional figure (Figure S1. ABCDE).

MTT Assay (Tetrazolium Reduction Assay)

The MTT assay was utilized to determine the cytotoxicity of various ZSM-5 and SBA-16 nanocarrier treatments on the A549 lung cancer cell line. The colorimetric dye-reduction method with 3-(4,5-dimethylthiazol-2-yl)-2,5-diphenyltetrazolium bromide was used to determine the number of live cells.

$$\text{Viability percentage} = \frac{A\text{Average T.OF Conc.} - \text{Average Blank}}{\text{Average of Control} - \text{Average Of Blank}} \; x \; 100\% \quad \ldots\ldots(2)$$

24 hours after the administration of the drugs. The suppression of cell proliferation was expressed as a percentage of the growth rate of the control cells. Each experiment was conducted three independent times. It has been used at various concentrations to treat cells, including 1.2, 0.9, 0.6, 0.3, and 0.1 M. The IC_{50} value was calculated by using the slope of the graph's equation. The results of the MTT test were calculated using equation 2 and the IC_{50} values for each type of carrier and free mebendazole were calculated.

At concentrations ranging from 0.1 to 1.2 M, studies on cell viability revealed that the blank (media) and control (DMSO) had no noticeable impact on A549 cells. The half-maximal inhibitory concentration (IC_{50}) for the first system, mebendazole loaded with ZSM-5, is 0.41M, while the IC_{50} for the coupling system is 0.48M. It was found, however, that another system, SBA-16 loaded MBZ, had an effect of 0.64 % at the half-maximal inhibitory concentration (IC_{50}),

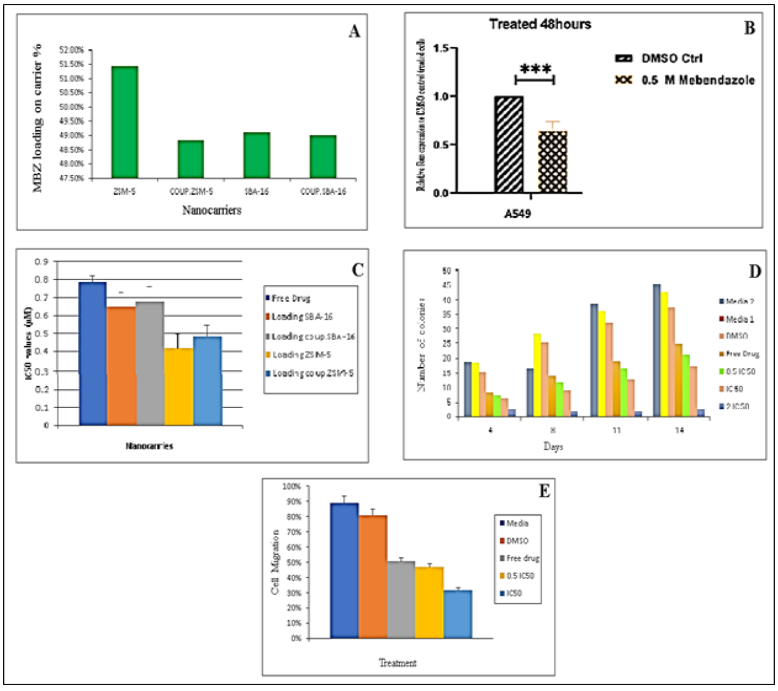

Figure 6: A) Forms of carrier loading drug B) PCR result: Ran expression was significantly down regulated C) the IC50 for each different forms of carriers and Free drug MTT assay result was calculated depended on viability percentage D) Growth of colonies after treatment The average of number of colonies were noticed and growth recorded according to the treatment was used E) Cell migration is showing that the ZSM-5 loaded drug treatment with cells migrate at a slower rate compared with the control cells (media and DMSO).

which was nearly equal to the effect of derivative coupling with SBA-16 loaded MBZ (IC_{50} = 0.68 percent).[64] Interestingly, the subsequent closing rate (IC_{50}) for the free drug mebendazole was 0.78%. Three independent 96-well MTT experiments were run, resulting in three distinct IC_{50} values for each carrier type and free drug. In addition, it has been demonstrated that the Ran-GTP inhibitor pimozide drastically reduces cell profiling (IC_{50} = 4.6 x 10-7 M).[65] This is consistent with our observations regarding mebendazole. In addition, the colony formation and migration assays revealed that co-loading mebendazole with ZSM-5 increased the inhibitory effect of mebendazole on the formation of treated cells compared to the carrier alone or on untreated cells. In addition, pimozide and another Ran inhibitor, peptide, significantly reduced colony formation and cell motility.[63] Fortunately, this is consistent with mebendazole's effect on colony formation and cell migration. From this study, it has been shown that ZSM-5 significantly enhances mebendazole's inhibitory effect on colony formation and cell migration. This explains the anti-invasive and anti-metastatic properties of mebendazole when added to the lung cancer cell line A549 that was treated in vitro with MBZ. In future studies, we will use an animal model system to determine whether mebendazole effectively prevents cancer spread (Supplementary Table 1-3).

Colony Assay (Triplicate Tests)

The colony test was used to determine the rate of expansion of cancer cells following therapy and the influence of untreated proliferation. A six-well plate was split, seeded on day 1, treated on day 2, removed on day 3, began counting on day 4, and kept counting expanding colonies on days 8, 11, and 14. The average number of colonies was noted, and growth was recorded according to the therapy employed; $2IC_{50}$ significantly slowed cell development when double the concentration of the medication was administered.[66] It was observed that the treatment with media and DMSO grew rapidly and densely, which was most likely due to the therapy's absence, as demonstrated in (Figure 4D). The X-axis represents the number of days counting colonies and the Y-axis represents the number of colonies. The graph demonstrates rapid growth in wells of media and DMSO due to the absence of treatment throughout the experiment. Even when treatment was used and removed, the effect of the drug slowed colony growth in all wells. According to double conc., the optimal outcome is $2IC_{50}$. By comparing free drug to loaded drug carriers, it has been demonstrated that carriers-drug coupled therapy has a greater impact than free drug by a lesser margin (IC_{50} and 0.5 IC_{50}).[61] The mean cell growth of 0.5 IC_{50} of C1, IC_{50} of C1,

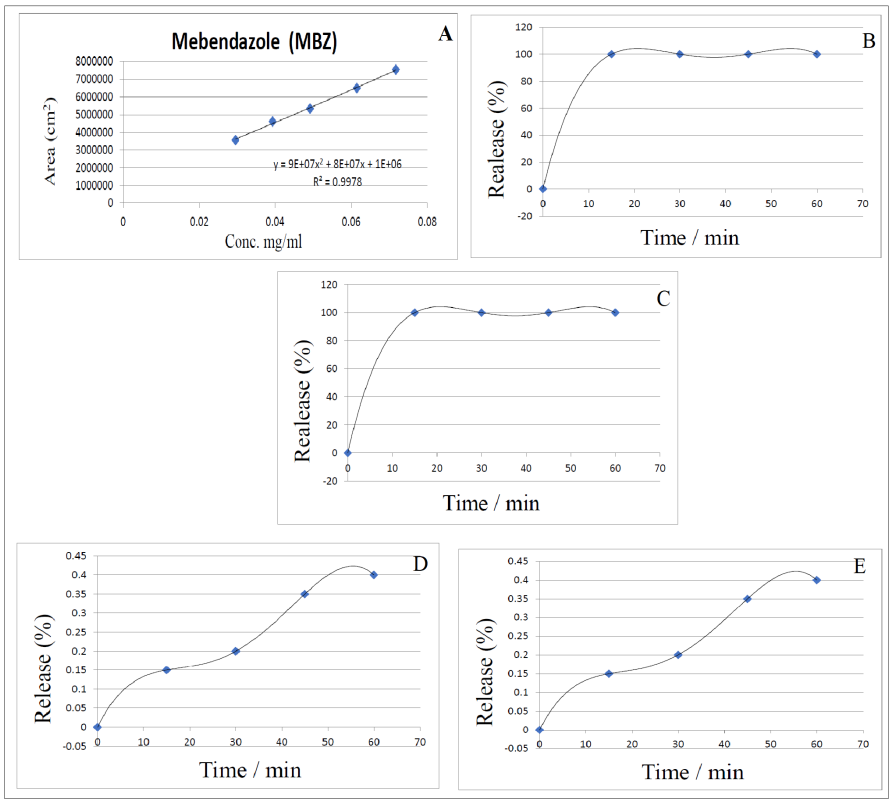

Fig. S1: A) Calibration curve of mebendazole B) Released % of Dissolution of Commercial Drug in HCL. C) Released % of Dissolution of Loaded Drug (carrier 1) in HCL. D) Released % of Dissolution of Commercial Drug in Buffer. E) Released % of Dissolution of Loaded Drug (carrier 1) in Buffer.

Supplementary Table 1: Infrared frequencies of the characteristic bands of ZSM-5 nanoparticles.

Group vibrations	*Wave number (cm ^{1})*
Si-OH-Al stretch	3366.6
H-O-H bend	1596.3
Si-O Asymmetric stretch	1096.8
Si/Al-O bend	1049.9
Si-O A symmetric stretch	926.5
Si-O-Al symmetry stretch	720
Al^{3+}	688.8

Supplementary Table 2: Infrared frequencies of the characteristic bands of SBA-16 nanoparticles.

Group vibrations	*Wave number (cm ^{1})*
Hydrogen-bonded Si-O-H and water	3292.8
Si-O-Si asymmetric stretching (external)	1199.6
Si-O stretching symmetric (external)	927
Si-O-Si asymmetric stretching (internal)	1049.9
Si-O-Si symmetric stretching (internal)	799.1
H-O-H bending	1596.7

and IC_{50} of C2 (M = 14.2500, SD = 6.07591), (M = 11.2500, SD = 4.78714), and (M = 2.2500, SD =.50000), respectively, was significantly less than Media 1 (control), (M = 29.2500, SD = 4.93039), with p values =0. 050, 0.041, and (Figure 4E, S2A).[67]

Migration Assay (Scratch)

Phase contrast is utilized to determine the percentage of closure, which reflects cell movement, and motic software is used to quantify the area between cell edges. On day 1, a six-well plate was divided and seeded. On days 2 and 3, the plate was treated and captured following treatment. The *in-vitro* scratch experiment (Figure 6D and S3) is shown to compare the effect of the medicines on the migration of the cell line A549. At the start and conclusion of a 24 hours incubation period, photographs revealed considerable migration of the cells toward the scratch. The incubation duration was set to 12 hours when the faster-moving cells (control, DMSO, and Media) were just about to close the scratch in 81.0 and 89.0 percent of the cases, respectively. The results for tracking migration of individual cells in the leading edge of the scratch using the in vitro scratch of (free drug, 0.5 IC_{50}, and IC_{50}) test were 50.5, 46.8, and 31.50%. The outcome of the image analysis. The photos revealed that the ZSM-5-loaded Melt-2015 treatment cells (denoted by arrows) moved more slowly than the control cells (media and DMSO).

The photographs below show a comparison of the areas two days after treatment; we noted that the area regularly dropped according to the conc. and controls, and that 2 IC 50 was the best result according to the double dosage control, as the effect was identified by Percent of Closure.[65]

PCR Polymerase Reaction

Supplementary Table 3:. Infrared frequencies of characteristic bands ofMebandazole and Mebandazole loaded SBA-16 and ZSM -5 nanoparticles.

Group Vibrations	Wave number (cm ^{1}) of	
	mebandazole	mebandazole loaded ZSM -5 and SBA-16
N-H	3484.32	Super imposed with Si-O-H, and Al-(OH)
C=O	1714.2	1716.8, 1716.8
C=N	1640.9	1641.7, 1642.0
C=C	1593.0	1594.1, 1593.7

qRT-PCR was used to determine the effect of mebendazole on Ran mRNA expression in lung A549 carcinoma cells. qRT-PCR was performed to assess Ran gene expression in response to mebendazole therapy. The cells were cultured and treated with 0.5M mebendazole for 48 hours. Cells were isolated and analyzed to determine the amount of Ran mRNA. Ran expression was considerably reduced in A549 p 0.001 cells treated with 0.5M mebendazole compared to the control. After 48 h, there was a considerable suppression of Ran mRNA of up to 40% in A549 cell line, as shown in (Figure 6 B).[49]

Percentage of closure = 100 - (area on day 2 / area on day 1) * 100%.....(3)

CONCLUSION

Hydrothermal preparation of mebendazole-loaded ZSM-5 and SBA 16 nanoparticles was used. The formulation drug is more effective than the unformulated drug. Carrier 1 (mebendazole loading ZSM-5) was demonstrated to be dependent on other tests owing to its higher loaded percent and significant IC50. The conclusion that our recipe outperformed the commercial-free drug in biological testing. In vitro viability experiments revealed that the first system (mebendazole loading ZSM-5) was much more cytotoxic than the free drug to lung cancer A549 cell line. Interestingly, the half-maximal inhibitory concentration 1/2 (IC50) for the first system ZSM-5 loading mebendazole is 0.41 M and 0.48 M for coupling ZSM-5, comparable with SBA!6 and coupling form were 0.64 and 0.68 respectively. In addition, the in vitro results have demonstrated that the efficiency of mebendazole loaded ZSM-5, SBA 16 and also coupling form of both nanocarriers against A549 lung cancer cell line, give significant reduction of IC50 compare with free drug.

Moreover, we conducted colony formation and migration assays, which It has been demonstrated that co-loading mebendazole with nano mesoporous carries improved the inhibitory impact of mebendazole on the biological cell properties including colony formation and immigration assay of treated cells. In contrast, it was no inhibitory effect of the carrier alone. Ran mRNA expression was significantly suppressed by up to 40% in the A549 cell line after treated

by mebendazole. This further demonstrates the in vitro anti-invasive effect of mebendazole mediated by inhibition of Ran expression. The significant findings of ZSM-5 nanoparticles in enhancing mebendazole's inhibitory effect on colony formation and cell migration may be used as in the future as a potential repurpose therapy for lung cancer.

CONTRIBUTIONS

H. E. carried out all experiments, data curation, software, and writing-original draft and F. M. contributed to supervision, validation, and review-editing. M. T. contributed to conceptualization, methodology, investigation, project administration, data validation, and writing-original draft.

GEOLOCATION INFORMATION

Acknowledgments

This work was supported by the scientific research -Al-Ahliyya Amman University

The a Pharmacological and Diagnostic Research Center. Faculty of Pharmacy Al-Ahliyya Amman, 19328, Jordan

FUNDING DETAILS

Disclosure Statement

The authors report there are no competing interests to declare.

Data Availability Statement

Data Deposition

REFERENCES

1. Johnson D. Treatment strategies for metastatic non–small-cell lung cancer. Clin Lung Cancer. 1999;1:34–41.
2. Utada M, Yonehara S, Ozasa K. Historical changes in histological diagnosis of lung cancer. J Epidemiol. 2018;29:238–240.
3. Gridelli C, Rossi A, Carbone D, et al. Non-small-cell lung cancer. Nat Rev Dis Primers. 2015;1:15009.
4. Osmani L, Askin F, Gabrielson E, et al. Current WHO guidelines and the critical role of immunohistochemical markers in the subclassification of non-small cell lung carcinoma (NSCLC): moving from targeted therapy to immunotherapy. Semin Cancer Biol. 2018;52:103–109.
5. Detterbeck F, Boffa D, Kim A, et al. The eighth edition lung cancer stage classification. Chest. 2017;151:193–203.
6. O'Neill A, Alessandrino F, Tirumani S, et al. Hallmarks of cancer in the reading room: a guide for radiologists. Am J Roentgenol. 2018;211:470–484.
7. Rotow J, Bivona T. Understanding and targeting resistance mechanisms in NSCLC. Nat Rev Cancer. 2017;17:637–658.
8. Adjei A. "Targeted" therapies for non-small-cell lung cancer. Clin Lung Cancer. 2002;4:124.
9. Kong L, Wang L, Xing L, et al. Current progress and outcomes of clinical trials on using epidermal growth factor receptor-tyrosine kinase inhibitor therapy in non-small cell lung cancer patients with brain metastases. Chronic Dis Transl Med. 2017;3:221–229.
10. Drilon A, Cappuzzo F, Ou S, et al. Targeting MET in lung cancer: will expectations finally be met? J Thorac Oncol. 2017;12:15–26.
11. Herbst R, Morgensztern D, Boshoff C. The biology and management of non-small cell lung cancer. Nature. 2018;553:446–454
12. Hanahan D, Weinberg RA. Hallmarks of cancer: the next generation. Cell. 2011;144:646–674.
13. Asao T, Takahashi F, Takahashi K. Resistance to molecularly targeted therapy in non-small-cell lung cancer. Respir Investig. 2019;57:20–26.
14. Imai K, Takaoka A. Comparing antibody and small-molecule therapies for cancer. Nat Rev Cancer. 2006;6:714–727.
15. Pakkala S, Ramalingam S. Personalized therapy for lung cancer: striking a moving target. JCI Insight. 2018;3.
16. Gschwind A, Fischer O, Ullrich A. The discovery of receptor tyrosine kinases: targets for cancer therapy. Nat Rev Cancer. 2004;4:361–370.
17. Haldar K, Gaitskell K, Bryant A, et al. Epidermal growth factor receptor blockers for the treatment of ovarian cancer. Cochrane Database Syst Rev. 2011;10:CD007927.
18. Machan R, Yavas S, Wohland T. The epidermal growth factor receptor forms location-dependent complexes in resting cells. Biophys J. 2016;111:2241–2254.
19. Linardou H, Dahabreh I, Bafaloukos D, et al. Somatic EGFR mutations and efficacy of tyrosine kinase inhibitors in NSCLC. Nat Rev Clin Oncol. 2009;6:352–366.
20. Hetzer M, Gruss O, and Mattaj I. The Ran GTPase as a marker of chromosome position in spindle formation and nuclear envelope assembly. Nat Cell Biol. 2002;4:E177–E184.
21. Ren M, Drivas G, D'Eustachio P, et al. Ran/TC4: a small nuclear GTP-binding protein that regulates DNA synthesis. J Cell Biol. 1993;120:313–323.
22. Fiore B, Ciciarello M, Lavia P. Mitotic functions of the Ran GTPase network: the importance of being in the right place at the right time. Cell Cycle. 2004;3:305–313.
23. Kalab P, Heald R. The RanGTP gradient–a GPS for the mitotic spindle. J Cell Sci. 2008;121:1577–1586.
24. Melchior F. Ran GTPase cycle: one mechanism—two functions. Curr Biol. 2001;11:R257–R260.
25. Wilde A, Zheng Y. Stimulation of microtubule aster formation and spindle assembly by the small GTPase Ran. Science. 1999;284:1359–1362.
26. Clarke P, Zhang C. Spatial and temporal coordination of mitosis by Ran GTPase. Nat Rev Mol Cell Biol. 2008;9:464–477.
27. Rensen W, Mangiacasale R, Ciciarello M, et al. The GTPase Ran: regulation of cell life and potential roles in cell transformation. Front Biosci. 2008;13:4097–4121.
28. Offit K. Personalized medicine: new genomics, old lessons. Hum Genet. 2011;130:3–14.
29. Xia F, Canovas P, Guadagno T, et al. A survivin-ran complex regulates spindle formation in tumor cells. Mol Cell Biol. 2008;28:5299–5311.
30. Trosko JE, Ruch RJ. Gap junctions as targets for cancer prevention and chemotherapy. Curr Drug Targets. 2002;3:465–482.
31. Moyano D, Rotello V. Nano meets biology: structure and function at the nanoparticle interface. Langmuir. 2011;27:10376–10385.
32. Danilczuk M, Dlugopolska K, Ruman T, et al. Molecular sieves in medicine. Mini Rev Med Chem. 2008;8:1407–1417.
33. Baudis S, Lendlein, Behl M. Cover picture: Macromol. Mater. Eng. 11/2014. Macromol Mater Eng. 2014;299:1292–1297.
34. Zhao D, Huo Q, Feng J, et al. Nonionic triblock and star diblock copolymer and oligomeric surfactant syntheses of highly ordered,

hydrothermally stable, mesoporous silica structures. J Am Chem Soc. 1998;120:6024–6036.
35. Tsotsalas M, Kopka K, Luppi G, et al. Encapsulating (111) in nanocontainers for scintigraphic imaging: synthesis, characterization, and in vivo biodistribution. ACS Nano. 2010;4:342–348.
36. Platas-Iglesias C, Vander Elst L, Zhou W, et al. Zeolite GdNaY nanoparticles with very high relaxivity for application as contrast agents in magnetic resonance imaging. ChemInform. 2003;34.
37. Ndiege N, Raidoo R, Schultz M, et al. Preparation of a versatile bifunctional zeolite for targeted imaging applications. Langmuir. 2011;27:2904–2909.
38. Arruebo M, Fernández-Pacheco R, Irusta S, et al. Sustained release of doxorubicin from zeolite-magnetite nanocomposites prepared by mechanical activation. Nanotechnology. 2006;17:4057–4064.
39. Braschi I, Gatti G, Paul G, et al. Sulfonamide antibiotics embedded in high silica zeolite Y: a combined experimental and theoretical study of host-guest and guest-guest interactions. Langmuir. 2010;26:9524–9532.
40. Hodali H, Marzouqa D. In vitro evaluation of zeolite nanoparticles as carrier for delivery of 5-fluorouracil. Asian J Chem. 2016;28:1479–1485.
41. Sonveaux P, Végran F, Schroeder T, et al. Targeting lactate-fueled respiration selectively kills hypoxic tumor cells in mice. J Clin Invest. 2008;118:3930–3942.
42. Hanafi-Bojd M, Ansari L, Malaekeh-Nikouei B. Codelivery of anticancer drugs and siRNA by mesoporous silica nanoparticles. Ther Deliv. 2016;7:649–655.
43. Zhang Y, Zhai M, Chen Z, et al. Dual-modified liposome codelivery of doxorubicin and vincristine improve targeting and therapeutic efficacy of glioma.. Drug Deliv. 2017;24:1045–1055.
44. Ieranò C, Portella L, Lusa S, et al. CXCR4-antagonist Peptide R-liposomes for combined therapy against lung metastasis. Nanoscale. 2016;8:7562–7571.
45. Thomas MJK, Slipper I, Walunj A, et al. Inclusion of poorly soluble drugs in highly ordered mesoporous silica nanoparticles. Int J Pharm. 2010;387:272–277.
46. Athens G, Shayib R, Chmelka B. Current opinion in colloid & interface science. Mater Sci. 2009;14:281–292.
47. Malhis A, Arar S, Fayyad M, et al. Amino- and thiol-modified microporous silicalite-1 and mesoporous MCM-48 materials as potential effective adsorbents for Pb(II) in polluted aquatic systems. Adsorp Sci Technol. 2017;36:270–286.
48. Y. Haggag, Y, M. Elshikh, M, M. El-Tanani, M, et al. Nanoencapsulation of sophorolipids in PEGylated ply(lactide-co-glycolide) as a novel approach to target colon carcinoma in the murine model. Drug Deliv Transl Res. 2020;10:1353–1366.
49. Cappiello F, Casciaro B, Mangoni ML. A novel in vitro wound healing assay to evaluate cell migration. JoVE. 2018;56825.
50. Yaparpalvi R, Loyalka SK, Tompson RV. Aerosol synthesis of spherical PbO particles. J Mater Sci Lett. 1994;13:749–751.
51. Harlick P, Tezel F. Adsorption of carbon dioxide, methane and nitrogen: pure and binary mixture adsorption for ZSM-5 with SiO2/Al2O3 ratio of 280. Separation and Purification Technology. 2003;33:199–210.
52. Shah TA, Din IM, Kanwal NF, et al. Direct synthesis of mesoporous molecular sieves of Ni-SBA-16 by internal pH adjustment method and its performance for adsorption of toxic brilliant green dye. Arab J Chem. 2015;8:579–586.
53. Thomas MJK, Slipper I, Walunj A, et al. Inclusion of poorly soluble drugs in highly ordered mesoporous silica nanoparticles. Int J Pharm. 2010;387:272–277.
54. Vadia N, Rajput S. Study on formulation variables of methotrexate loaded mesoporous MCM-41 nanoparticles for dissolution enhancement. Eur J Pharm Sci. 2012;45:8–18.
55. Barbera´ A, Lorenzo N, Domı´nguez C. Biotecnologı´a Aplicada. 2012;29:146–154.
56. Khezri K, Haddadi-Asl V, Roghani-Mamaqani H. Nano. 2014;9:1450023.
57. Arias L, López-Viota M, Clares B, et al. J Pharm Sci. 2008;34:257–262.
58. Hassanpour S, Taghizadeh M, Yaripour F. Preparation, characterization, and activity evaluation of H-ZSM-5 catalysts in vapor-phase methanol dehydration to dimethyl ether. Ind Eng Chem Res. 2010;49:4063–4069.
59. Wu S-H, Hung Y, Mou C-Y. Mesoporous silicananoparticles as nanocarriershem Commun. 2011;47:9972.
60. Chen CY, Ouyang X, Zones SI, et al. Corrigendum to "characterization of shape selective properties of zeolites via hydroisomerization of n-hexane" [Micropor. Mesopor. Mater. 164 (2012) 71–81]. Micropor Mesopor Mater. 2013;169:248.
61. Brusau, E, Camí, G, Narda, G, Cuffini, S, Ayala, A, and Ellena, J. Synthesis and Characterization of a New Mebendazole Salt: Mebendazole Hydrochloride. Journal of Pharmaceutical Sciences. 2008;97:542–552.
62. Lin FH, Lee YH, Jian CH, et al. A study of purified montmorillonite intercalated with 5-fluorouracil as drug carrier. Biomaterials. 2002;23:1981–1987.
63. Huang MH, Choudrey A, Yang P. Ag nanowire formation within mesoporous silica. Chem Commun. 2000;1063–1064.
64. Guerini AE, Triggiani L, Maddalo M, et al. Mebendazole as a Candidate for Drug Repurposing in Oncology: An Extensive Review of Current Literature. Cancers (Basel).
65. Yuen H, Chan K, Platt-Higgins A, et al. Ran GTPase promotes cancer progression via Met receptor-mediated downstream signaling. Oncotarget. 2016;7:75854-75864.(9):1284. Published 2019 Aug 31. doi:10.3390/cancers11091284
66. Franken NAP, Rodermond HM, Stap J, et al. Clonogenic assay of cells in vitro. Nat Protoc. 2006;1:2315–2319.
67. Rushworth, L. K., Hewit, K., Munnings-Tomes, S., Somani, S., James, D., Shanks, et., al. Repurposing screen identifies mebendazole as a clinical candidate to synergise with docetaxel for prostate cancer treatment. British journal of cancer,. 2020;122: 517–527.
68. Haggag Y, Matchett K, Dakir E, et al. Nano-encapsulation of a novel anti-Ran-GTPase peptide for blockade of regulator of chromosome condensation (RCC1) function in MDAMB-231 breast cancer cells. Int J Pharm. 2017;521:40–53.